A THEORETICAL INVESTIGATION OF THE COUPLING OF PLATE TECTONICS AND MANTLE FLOW INDUCED BY THE FORCES AND MOTIONS OF ACTIVE (SLAB CONNECTED) PLATES

A THESIS SUBMITTED TO THE GRADUATE DIVISION OF THE UNIVERSITY OF HAWAII IN PARTIAL FULFILLMENT OF THE REQUIREMENTS FOR THE DEGREE OF

MASTER OF SCIENCE

IN

GEOLOGY AND GEOPHYSICS

DECEMBER 1996

By

William Bruce Paulk

Thesis Committee:

David Bercovici, Chairperson
Richard Hey
Pal Wessel

We certify that we have read this thesis and that, in our opinion, it is satisfactory in scope and quality as a thesis for the degree of Master of Science in Geology and Geophysics.

THESIS COMMITTEE

Chairperson

ACKNOWLEDGMENTS

Always first, I thank my Lord and Savior for giving me the necessary patience and perseverance, that of myself I do not have, to complete this work.

I especially want to thank my beautiful, loving and hard working wife Enid. Enid has handled details of our lives that are too numerous to mention and without her I could not have completed this program.

I am especially grateful and thankful to have worked with David Bercovici my advisor and committee chairman. In addition to being an extremely easy person to work with, Dave has given me so much useful advice necessary for the completion of this work. The contents of this thesis are heavily influenced by Dave's theoretical perspective and his studies. I can not thank him enough.

I want to thank Pal Wessel for patiently helping me with some of my earlier difficulties in getting started on the computer system and some basic understanding of geophysical data analysis.

I want to thank Richard Hey for his excellent presentation of the basics of plate tectonics.

I deeply appreciate all the help and advice given by my committee members and also want to thank everyone in the SOEST community that helped me with my studies and made my time here very interesting and enjoyable.

ABSTRACT

The tectonic plates are presumably driven by some form of thermal convection process. In particular, historic studies have shown that slab connected plates are the most active. However, these studies have not shown quantitatively whether the more active slab connected plates drive the passive plates. We will show that passive plates that are adjacent to convergent margins are driven by the active plates. Using a three dimensional viscous flow in a spherical shell, we determine how mantle flow is driven by active plates. The traction on the base of the passive plates, due to this mantle flow, is then used to infer how much of the motion of the passive plates is caused indirectly by the active plates for both the free slip bottom boundary (Earth's core) and no slip shallow boundary (660 kilometer discontinuity) cases.

TABLE OF CONTENTS

TABLE OF CONTENTS

LIST OF TABLES

LIST OF FIGURES

Chapter 1

TRACTION AND TORQUE STUDY OF THE EFFECT OF THE ACTIVE PLATES ON THE PASSIVE PLATES

1.1 SUMMARY

Five of the twelve plates (Cocos, Indian, Nazca, Pacific and Philippine) are much more active than the other seven and are named the *active plates.* These plates all have massive connecting slabs which account for the largest plate driving forces (slab pull) and cause the greatest plate velocities (Forsyth and Uyeda, 1975; Hager and O'Connell, 1981). The slabs can only pull the plates they are attached to, which is in accordance with the greater picture of a downwelling mantle driven from within by heat generated from radiogenic sources (Bercovici, Schubert and Glatzmaier, 1989). Ridges do not create driving forces of any consequence and are only the surface effect of weakly upwelling mantle material filling the void left by plates that are diverging. The remaining plate boundaries are either in collision or moving relative to each other and can only offer resistance. This study will show that the flow driven in the mantle by the five active plates is accountable for the motion and direction of some of the seven remaining plates that are adjacent to slab connected margins. These seven much less active plates (African, Antarctic, Arabian, Caribbean, Eurasian, North American and South American) are called the *passive plates.*

1.2 HISTORICAL BACKGROUND

The motivation for investigating whether the motion of the active plates will move the passive plates via mantle flow comes from a variety of earlier studies.

The classic *Rayleigh-Benard* experiment is one of the earliest attempts to study the

physics of convection. The first experiments were performed in the early 1900's and were concerned with the motion of horizontal layers of fluid heated from below (Chandrasekhar, 1981). When fluid is heated from below, it becomes less dense than the fluid above and becomes unstable. However, a fluid offers internal resistance prior to being displaced. Internal resistance is due to the viscosity of the fluid which damps out motion until the thermal buoyancy is high enough to overcome viscous effects. Once the fluid is in motion, it forms convection cells. Analogously, the tectonic plates at the Earth's surface are thought to be the visible emerging and descending upper surface of convecting cells.

Observations concerning plate velocities and the length of subducting slabs have shown that the plates do not behave consistently with the premise that convection cells drive all spreading centers and subduction zones. A study confirming excellent correlation between plate velocities and the lengths of subducting slabs was developed by accounting for all the forces acting on the twelve plates and their geometry (Forsyth and Uyeda, 1975). I.e., forces such as basal drag, ridge push and slab pull were also included. In addition, the forces due to the slabs were balanced by including viscous stress resistance from the mantle.

Forsyth and Uyeda (1975) concluded that the greatest forces acting on the plates are due to descending slabs and that these forces are responsible for the greater plate velocities of the active plates. Subduction does not occur as a result of a slab being pulled down by a convection cell, but because the slab is the sinking portion of the convecting cell.

In an effort to study the larger scale flow of the mantle in conjunction with plate motion, Hager and O'Connell (1978) developed a kinematic model using the observed plate geometry and velocities as boundary conditions to simulate large scale flow. Their kinematic model revealed a strong relationship or correlation (.99) between the dip of seismic *Benioff* zone and the modeled trajectory of subducting slabs, if the flow was allowed to extend below 700 km (possibly the 660 km discontinuity) and into the lower mantle.

Hager and O'Connell (1978) concluded that the high correlation between the seismic and modeled slabs revealed that the dip of a subducting slab is determined by the large scale flow induced by a plate translating and that convection is not confined to the upper mantle. This study, in addition to the Forsyth and Uyeda (1975) study, suggests that the slab connected tectonic plates drag the mantle and thus, could have an effect on the motion of adjacent plates.

Later, Hager and O'Connell (1981) completed a study consisting of a model of a plastic lithosphere overlaying an asthenosphere composed of a viscous *Newtonian* fluid. Their model includes changes in density and body forces of a cooling lithosphere moving away from a source. In addition, their model contains continental and oceanic density variations and plate velocities complete with plate shapes, the stresses at the surface created by the suction and the viscous shear of the flow on the subducting slabs. Their study was based on a spherical geometric solution of the *Navier-Stokes* equation for the actual plate geometry while using the net force on the plates due to the subducting slabs.

Hager and O'Connell (1981) concluded, as did Forsyth and Uyeda (1975), that slabs were responsible for the largest forces transmitted to plates. They also calculated the forces due to ridge push and density changes in the lithosphere moving away from a ridge and concluded that the next most significant force transmitted to plates was due to the density changes in the moving lithosphere. In addition, they claimed that density changes are essentially independent of the rheology of the lithosphere, that the driving force from thickening with age is not influenced by viscosity changes and that the forces resisting slab pull and density changes in the athenosphere are largely due to basal drag and convergent and frictional forces on plate boundaries.

In all the studies, the spherical harmonic models of plate motions are plagued with the problem of singularities in the horizontal divergence and vorticity due to discontinuity of the plate boundary at the surface. Where discontinuous plate boundaries exist, which in

turn creates discontinuous velocities, basal traction becomes infinitely great. I.e., extreme basal traction is not a measure of realistic physical conditions and indicates that a different approach to this problem is needed.

In an effort to solve the discontinuity problem in plate and mantle coupling, Bercovici and Wessel (1994) developed a kinematic plate model that is infinitely differentiable. Their model removed the discontinuity between the plates and the mantle by allowing an area or margin where, as at the Earth's surface, plate deformation takes place. Their shape function is offered as a solution to the discontinuity problem, is mathematical in concept and does not infer that any real physical model is used.

In conclusion, there have been many studies to examine the motion between convecting cells and tectonic plates. The majority of these studies recognize that slab pull is the major driving force and is the cause of the greater plate velocities of the active plates. This is in accordance with the present theory of mantle convection, where strong downwellings and weak upwellings of the mantle are caused by a mantle heated by radiogenic sources from within. However, these studies have not shown quantitatively whether the more active slab connected plates drive the passive plates. This investigation will show that the passive plates adjacent to the slab connected plates or converging plate margins are driven by the traction produced by the mantle on the underside of the passive plates.

1.3 TRACTION AND TORQUE STUDY

We wish to examine the extent to which the flow driven in the mantle by the motion of the five active plates drive the seven passive plates by accomplishing a series of steps:

We will use plate boundary data (Minster and Jordan, 1980), plate angular velocity data from the NUVEL-1 Pacific-plate-fixed Euler poles (DeMets et al., 1990) and the instantaneous Hotspots-Pacific pole added to the NUVEL-1 poles (Pollitz, 1988) which

have been consolidated into one filtered data set complete with continuously shaped plate boundaries that have been transformed into a colatitude-longitude grid for all of the plates (Bercovici and Wessel, 1994).

We will solve the viscous spherical shell problem, allowing the passive plates to be driven by the flow of the mantle induced by the active plates only. I.e., the active plates will be allowed to move and the passive plates will be held rigid.

We will determine the viscous traction beneath the passive plates to obtain the net torque on these plates.

We will compare the modeled torque calculations on both the active and passive plates to the individual observed torque on each of the plates. The individual observed torque on each plate is calculated by holding all the plates rigid except the plate which will be used for the comparison with the model.

We will make the above comparison for two separate depths in the mantle. I.e., we will be comparing the torque on all the passive plates to the torque for the individual plates for flow extending to the Earth's core mantle boundary and to the shallower 660 kilometer discontinuity. The core mantle boundary is considered to be a free slip boundary since the outer core is molten. We treat the 660 kilometer discontinuity as a no slip boundary for models where the lower mantle has a much higher viscosity than the upper mantle.

Our problem is simplified by using a kinematic model and neglecting the effects of temperature on the mantle's density and viscosity. As the mantle is very viscous, the plates are in dynamic equilibrium and that the net torque on the system is zero. On the negative side, we lose any knowledge of driving forces as the dynamics of the model no longer exist when the equation of motion is decoupled from the energy equation. On the positive side, we can treat the mantle as an essentially homogenous, isotropic material by not further complicating the flows. Thus, our flow model rheology will be a *Newtonian* fluid.

1.4 REFERENCES

Bercovici, D. and P. Wessel, A continuous kinematic model of plate-tectonic motions, *Geophys. J. Int.*, **119**, 595-610, 1994.

Bercovici, D., G. Schubert, and G. Glatzmaier, Three-dimensional spherical models of convection in the Earth's mantle, *Science*, **244**, 950-955, 1989.

Chandrasekhar, S., *Hydrodynamic and Hydromagnetic Stability*, 652 pp., Dover Publications, New York, 1961.

DeMets, C., R. Gordon, D. Argus and S. Stein, Current plate motions, *Geophys. J. Int.*, **101**, 425-478, 1990.

Forsyth, D. and S. Uyeda, On the relative importance of the driving forces of plate motion, *Geophys. J. R. astr. Soc.*, **43**, 163-200, 1975.

Hager, B., and R. O'Connell, Subduction zone dip angles and flow driven by plate motions, *Tectonophysics*, **50**, 111-33, 1978.

Hager, B., and R. O'Connell, A simple global model of plate dynamics and mantle convection , *J. geophys Res.*, **86**, 4843-67, 1981.

Minster, J., and T. Jordan, Present-day plate motions, *J. geophys. Res.*, **83**, 5331-54, 1978.

Pollitz, F., Episodic North America and Pacific plate ,motions, *Tectonics*, **7**, 711- 26, 1988.

Chapter 2
THEORETICAL EQUATIONS

2.1 SUMMARY

We will develop the theoretical equations required to calculate the global viscous horizontal traction field produced by the five active plates on the seven passive plates near the Earth's surface for a free slip bottom boundary (the Earth's core) and a no slip shallow boundary (the 660 km discontinuity).

2.2 CONTINUITY AND VELOCITY EQUATIONS

For our model, we assume that the Earth's mantle is an incompressible fluid. For an incompressible fluid, the requirement of continuity or no divergence must be satisfied. The continuity equation is

$$\nabla.\mathbf{v} = 0 \tag{1}$$

where $\mathbf{v}$ is the velocity vector at any position within the fluid. Chandrasekhar (1981) defines the velocity as the sum of two solenoidal vector fields which satisfy equation (1):

$$\mathbf{v} = \nabla\times\nabla\times\left[W(r,\vartheta,\varphi)\mathbf{r}\right] + \nabla\times\left[Z(r,\vartheta,\varphi)\mathbf{r}\right] \tag{2}$$

where $W(r,\vartheta,\varphi)$ is the poloidal potential, $Z(r,\vartheta,\varphi)$ is the toroidal potential, $\mathbf{r}$ is the radial position vector and r is the radius at any position within a sphere of colatitude: ϑ and longitude: φ. These potentials will be discussed in detail in the following sections.

The radial, colatitudinal and longitudinal velocity components are

$$v_r = \frac{L^2 W(r,\vartheta,\varphi)}{r} \tag{3}$$

$$v_\vartheta = \frac{1}{r}\frac{\partial^2\left(W(r,\vartheta,\varphi)r\right)}{\partial r\partial\vartheta} + \frac{1}{\sin\vartheta}\frac{\partial Z(r,\vartheta,\varphi)}{\partial\varphi} \tag{4}$$

$$v_\varphi = \frac{1}{r\sin\vartheta}\frac{\partial^2\left(W(r,\vartheta,\varphi)r\right)}{\partial r\partial\varphi} - \frac{\partial Z(r,\vartheta,\varphi)}{\partial\vartheta}, \tag{5}$$

respectively. The angular momentum operator equation is

$$L^2 = -\frac{1}{\sin\vartheta}\frac{\partial}{\partial\vartheta}\left(\sin\vartheta\frac{\partial}{\partial\vartheta}\right) - \frac{1}{\sin^2\vartheta}\frac{\partial^2}{\partial\varphi^2} \tag{6}$$

(Chandrasekhar, 1981).

2.3 THE EQUATION OF MOTION

We require an equation to describe the motion of the convective system which we assume consists of a viscous fluid. The general form of the equation of motion for a viscous fluid (the *Navier-Stokes equation*) is

$$\rho\left(\frac{\partial v_i}{\partial t} + v_j\frac{\partial v_i}{\partial x_j}\right) = -\frac{\partial p}{\partial x_i} + \rho g_i + \frac{\partial}{\partial x_j}\left[2\mu e_{ij} - \frac{2}{3}\mu(\nabla.\mathbf{v})\delta_{ij}\right] \tag{7}$$

where ρ is the density, v_i is the *i*th velocity component, p is the pressure, g_i is the sum of

$$e_{ij} = \frac{1}{2}\left(\frac{\partial v_i}{\partial x_j} + \frac{\partial v_j}{\partial x_i}\right)$$

the body forces, μ is the viscosity and the shear strain-rate tensor is

(Kundu, 1990; Landau and Lifshitz, 1987).

We assume viscosity is not temperature dependent. Therefore, μ is treated as a constant and can be taken outside of the derivative in equation (7). As stated earlier, if the fluid is incompressible, the velocity field is solenoidal and the divergence of the velocity or $\nabla.\mathbf{v}$ will vanish from the equation. Also, if the fluid is highly viscous, then acceleration and inertia are negligible and the material derivative on the left side of the equation vanishes. Thus, the reduced equation of motion for our model is

$$-\nabla p + \rho\mathbf{g} + \mu\nabla^2\mathbf{v} = 0$$

(8)

where the only body force contained in our model is gravity or g(r). We also assume that ρ is a constant. The observed velocities on the surface of the Earth that are produced by unknown forces will be introduced via the boundary conditions in a later section.

2.4 VORTICITY AND BIHARMONIC EQUATIONS

To solve the reduced equation of motion, we take the dot product of **r** with the curl of equation (8) and substitute equation (2) for **v**. Both the gravity and pressure can be expressed as gradients of a scalar and vanish under a curl. The vorticity equation for $Z(r,\vartheta,\varphi)$ is

$$\nabla^2\mathbf{r}.\nabla\times\mathbf{v} = \nabla^2\left[L^2 Z(r,\vartheta,\varphi)\right] = 0. \tag{9}$$

Analogously, we take the dot product of **r** with the curl of the curl of equation (8) and substitute equation (2) for **v**. The gravity and pressure terms again vanish under this equation and the biharmonic equation for $W(r,\vartheta,\varphi)$ is

$$\nabla^2\mathbf{r}.\nabla\times\nabla\times\mathbf{v} = -\nabla^4\left[L^2 W(r,\vartheta,\varphi)\right] = 0. \tag{10}$$

We will require spherical harmonic solutions to satisfy equations (9) and (10). The normalized spherical harmonic representation of $W(r,\vartheta,\varphi)$ is

$$W(r,\vartheta,\varphi) = \sum_{l=0}^{\infty}\sum_{m=-l}^{+l} W_l^m(r) Y_l^m(\vartheta,\varphi) \tag{11}$$

where $Y_l^m(\vartheta,\varphi) = (-1)^{|m|}\sqrt{\dfrac{2l+1}{4\pi}\dfrac{(l-|m|)!}{(l+|m|)!}}P_l^m(\cos\vartheta)e^{im\varphi}$ is the normalized spherical harmonic (Arfken, 1985), $P_l^m(\cos\vartheta)$ is the *associated Legendre function* or colatitudinal component, $e^{im\varphi}$ is the longitudinal component and the radial component with complex coefficients which satisfies equation (10) is

$$W_l^m(r) = A_{lm}^{(1)} r^l + A_{lm}^{(2)} r^{-(l+1)} + A_{lm}^{(3)} r^{l+2} + A_{lm}^{(4)} r^{-(l-1)}. \tag{12}$$

The normalized spherical harmonic representation of $Z(r,\vartheta,\varphi)$ is

$$Z(r,\vartheta,\varphi) = \sum_{l=0}^{\infty}\sum_{m=-l}^{+l} Z_l^m(r) Y_l^m(\vartheta,\varphi) \tag{13}$$

where the radial component with complex coefficients which satisfies equation (9) is

$$Z_l^m(r) = B_{lm}^{(1)} r^l + B_{lm}^{(2)} r^{-(l+1)}. \tag{14}$$

Note we have used the identity that $L^2 Y_l^m = l(l+1)Y_l^m$.

2.5 BOUNDARY CONDITIONS

Certain boundary conditions are applied to the plates and mantle to solve the viscous shell problem. These conditions apply at the surface and at an inner radius of a sphere (Chandrasekhar, 1981). The driving forces for our model will be introduced near the Earth's surface or outer radius and free slip or no slip boundary conditions will be introduced at the Earth's core mantle boundary or 660 km discontinuity inner radii of the sphere, respectively.

2.5.1 Spherical Surface Boundary

At the spherical surface, no radial component of velocity can exist. Therefore, $v_r\big|_{r=R_o} = 0$ where R_o is the outer radius of the sphere. I.e., no radial poloidal contribution can exist at the surface, which is equivalent to

$$W_l^m(r)\big|_{r=R_o} = 0. \tag{15}$$

However, the horizontal velocity components; v_ϑ and v_φ do exist at the surface. Therefore, $\dfrac{\partial\left(W_l^m(r)r\right)}{\partial r}$ and $Z_l^m(r)$ do not vanish. To introduce the observed surface conditions that are produced by the driving forces of the system, we will use the horizontal divergence and the radial vorticity relationships in the Bercovici and Wessel, (1994) model, but where only active plates move, to solve for $\dfrac{\partial\left(W_l^m(r)r\right)}{\partial r}$ and $Z_l^m(r)$. The horizontal divergence at the surface is

$$D = \nabla_h \cdot \mathbf{v} \tag{16}$$

where the horizontal operator is

$$\nabla_h = \left(0, \frac{1}{r}\frac{\partial}{\partial\vartheta}, \frac{1}{r\sin\vartheta}\frac{\partial}{\partial\varphi}\right). \tag{17}$$

and the spherical harmonic expansion is

$$D = \sum_{lm} D_{lm} Y_l^m. \tag{18}$$

The radial vorticity at the surface is

$$\omega_r = \hat{r}.\nabla \times \mathbf{v} \tag{19}$$

and the spherical harmonic expansion is

$$\omega_r = \sum_{lm} \omega_{lm} Y_l^m. \tag{20}$$

Equations (2), (17) and (18) are substituted into equation (16) to solve for $\frac{\partial(W_l^m(r)r)}{\partial r}$ at the surface, obtaining

$$\left.\frac{\partial(W_l^m(r)r)}{\partial r}\right|_{r=R_o} = -\frac{R_o^2}{l(l+1)} D_{lm} \tag{21}$$

where $l = 1,2,3,....,\infty$ and $m = -l,-l+1,...,l-1,l$. Similarly, equations (2) and (20) are substituted into equation (19) to solve for $Z_l^m(r)$ at the surface, obtaining

$$Z_l^m(r)\big|_{r=R_o} = \frac{R_o}{l(l+1)} \omega_{lm}. \tag{22}$$

2.5.2 Lower Boundaries

Two of the Earth's inner radii will be considered. The radius of the Earth's core is a natural bottom boundary for mantle material between the mantle and the liquid outer core. Therefore, we would expect the interface to be nonrigid, defining a free slip boundary. If the Earth's core is the only interior boundary, only one convective layer of mantle exists. Conversely, the shallow boundary at a lesser depth of 660 kilometers is not necessarily between two different mantle materials. I.e., the interface between these materials is possibly approximately rigid if the lower mantle is much more viscous than the upper mantle; this defines a no slip boundary and suggests an additional layer or a double layer convective system (Hager and O'Connell 1978; Hager and O'Connell 1981). We do not know if there are one or two layers of large-scale convection. However, we will confine our study to behavior at the Earth's surface, while using either the free slip or the no slip

boundaries to determine which model boundary condition yields the most consistent results when compared to observable conditions at the surface.

At either the free slip or the no slip boundaries, as at the Earth's surface, no radial velocity component can exist. Therefore, $v_r\big|_{r=R_i} = 0$ where R_i is the inner radius of the inner boundary. Nonexistent radial velocity is equivalent to

$$W_l^m(r)\big|_{r=R_i} = 0. \tag{23}$$

At the free slip bottom boundary, tangential viscous stresses are nonexistent. The absence of these stresses requires that $\sigma_{R_i\vartheta} = 0$ and $\sigma_{R_i\varphi} = 0$, or equivalently that

$$\left.\frac{\partial^2 W_l^m(r)}{\partial r^2}\right|_{r=R_i} = \left.\frac{\partial}{\partial r}\left(\frac{Z_l^m(r)}{r}\right)\right|_{r=R_i} = 0. \tag{24}$$

and (25)

See Chandresekhar (1981). The derivation of equations (24) and (25) is essentially the same as the steps between equations (36) through (40) in section 2.7.2, with the exception that equations (39) and (40) would be equal to zero at the free slip bottom boundary.

At the no slip shallow boundary, colatitudinal or longitudinal velocity components are nonexistent . Thus, $v_\vartheta\big|_{r=R_i} = v_\varphi\big|_{r=R_i} = 0$. Therefore,

$$\left.\frac{\partial W_l^m(r)}{\partial r}\right|_{r=R_i} = Z_l^m(r)\big|_{r=R_i} = 0\ . \tag{26) and (27}$$

2.6 COMPLEX COEFFICIENTS

With the boundary conditions at the Earth's surface and inner radii established, the determination of the complex coefficients in equations (12) and (14) reduces to finding the solutions to matrix equations.

2.6.1 Coefficients for a Free Slip Boundary

The matrix equation used to solve for the poloidal complex coefficients in equations (15), (21), (23) and (24) is

$$\begin{bmatrix} R_o^l & R_o^{-(l+1)} & R_o^{l+2} & R_o^{-(l-1)} \\ R_i^l & R_i^{-(l+1)} & R_i^{l+2} & R_i^{-(l-1)} \\ l(l-1)R_i^{l-2} & (l+1)(l+2)R_i^{-(l+3)} & (l+1)(l+2)R_i^l & l(l-1)R_i^{-(l+1)} \\ (l+1)R_o^l & -lR_o^{-(l+1)} & (l+3)R_o^{l+2} & -(l-2)R_o^{-(l-1)} \end{bmatrix} \begin{bmatrix} A_{lm}^{(1)} \\ A_{lm}^{(2)} \\ A_{lm}^{(3)} \\ A_{lm}^{(4)} \end{bmatrix} =$$

$$\begin{bmatrix} 0 \\ 0 \\ 0 \\ \dfrac{-R_o^2}{l(l+1)} D_{lm} \end{bmatrix}$$

(28)

and the matrix equation used to solve for the toroidal complex coefficients in equations (22) and (25) is

$$\begin{bmatrix} (l-1)R_i^{l-2} & -(l+2)R_i^{-(l+3)} \\ R_o^l & R_o^{-(l+1)} \end{bmatrix} \begin{bmatrix} B_{lm}^{(1)} \\ B_{lm}^{(2)} \end{bmatrix} = \begin{bmatrix} 0 \\ \dfrac{R_o}{l(l+1)} w_{lm} \end{bmatrix}. \tag{29}$$

2.6.2 Coefficients for a No Slip Boundary

The matrix equation used to solve for the poloidal complex coefficients in equations (15), (21), (23) and (26) is

$$\begin{bmatrix} R_o^l & R_o^{-(l+1)} & R_o^{l+2} & R_o^{-(l-1)} \\ R_i^l & R_i^{-(l+1)} & R_i^{l+2} & R_i^{-(l-1)} \\ lR_i^{l-1} & -(l+1)R_i^{-(l+2)} & (l+2)R_i^{l+1} & -(l-1)R_i^{-l} \\ (l+1)R_o^l & -lR_o^{-(l+1)} & (l+3)R_o^{l+2} & -(l-2)R_o^{-(l-1)} \end{bmatrix} \begin{bmatrix} A_{lm}^{(1)} \\ A_{lm}^{(2)} \\ A_{lm}^{(3)} \\ A_{lm}^{(4)} \end{bmatrix} =$$

$$\begin{bmatrix} 0 \\ 0 \\ 0 \\ \dfrac{-R_o^2}{l(l+1)} D_{lm} \end{bmatrix} \tag{30}$$

and the matrix equation for the toroidal complex coefficients in equations (22) and (27) is

$$\begin{bmatrix} R_i^l & R_i^{-(l+1)} \\ R_o^l & R_o^{-(l+1)} \end{bmatrix} \begin{bmatrix} B_{lm}^{(1)} \\ B_{lm}^{(2)} \end{bmatrix} = \begin{bmatrix} 0 \\ \dfrac{R_o}{l(l+1)} w_{lm} \end{bmatrix}. \tag{31}$$

2.7 TORQUE AND TRACTION EQUATIONS

Mantle flow induced by motion of active plates causes traction on the base of the passive plates. Thus, we require the equations for the traction exerted by the mantle on the passive plates.

2.7.1 Basic Torque Equations

The moment of a force or a system of forces that cause rotation is given by the torque vector; **T**. The general form of the equation for the torque vector at any position in space is

$$\mathbf{T} = \int \mathbf{R} \times \mathrm{d}\mathbf{F} \tag{32}$$

where the position vector is **R** and the force element acting at any position in space is d**F**. With $\mathrm{d}\mathbf{F} = \left(\underline{\underline{\mathbf{t}}}_s \cdot \hat{n}\right) dA$ and $\mathbf{R} = R_o \hat{r}$, the torque associated with the sum of the forces acting on any shell (tectonic plate) near the surface of a sphere is

$$\mathbf{T} = \int_s R_o \hat{r} \times \left(\underline{\underline{\mathbf{t}}}_s \cdot \hat{n}\right) dA \tag{33}$$

where R_o is the radius of the sphere, $\underline{\underline{\mathbf{t}}}_s$ is the stress tensor, $\hat{n}$ is the unit normal to the plate and $dA = R_o^2 \sin\vartheta d\vartheta d\varphi$ is the area element on a spherical surface.

We substitute the area element into equation (33), then for the *i*th plate we have

$$\mathbf{T}^{(i)} = R_o^3 \int_0^{\pi} \int_0^{2\pi} \hat{r} \times \left(\underline{\underline{\mathbf{t}}}_s \cdot \hat{n}\right) S^{(i)}(\vartheta, \varphi) \sin\vartheta d\vartheta d\varphi \tag{34}$$

where i = 1,2,3,....,12 and $S^{(i)}(\vartheta, \varphi)$ is the shape function for each plate.

2.7.2 Stress and Traction Equations

Given the previous section, solutions for the stress tensor are required to develop the proper torque. The constitutive equation for the stress tensor in a Newtonian fluid is

$$\underline{\underline{\mathbf{t}}}_s = -p\underline{\underline{\mathbf{I}}} + \underline{\underline{\sigma}} \tag{35}$$

where p is the pressure, $\underline{\underline{\mathbf{I}}}$ is the identity tensor and $\underline{\underline{\sigma}}$ is the deviatoric stress tensor (Kundu, 1990).

The deviatoric stress tensor equation for an incompressible viscous fluid is

$$\sigma_{ij} = -p\delta_{ij} + \mu\left(\frac{\partial v_i}{\partial x_j} + \frac{\partial v_j}{\partial x_i}\right) \tag{36}$$

and the stress tensor component equations in radial directions in spherical polar coordinates are

$$\sigma_{r\vartheta} = \mu\left[r\frac{\partial}{\partial r}\left(\frac{v_\vartheta}{r}\right) + \frac{1}{r}\frac{\partial v_r}{\partial \vartheta}\right] \tag{37}$$

$$\sigma_{r\varphi} = \mu\left[r\frac{\partial}{\partial r}\left(\frac{v_\varphi}{r}\right) + \frac{1}{r\sin\vartheta}\frac{\partial v_r}{\partial \varphi}\right] \tag{38}$$

(Landau and Lifshitz, 1987).

At the surface of the sphere, radial components of velocity are nonexistent. Therefore, $v_r|_{r=R_o} = \left.\frac{\partial v_r}{\partial \vartheta}\right|_{r=R_o} = \left.\frac{\partial v_r}{\partial \varphi}\right|_{r=R_o} = 0$ and the only stresses that cause motion in the ϑ or φ directions are

$$\sigma_{R_o\vartheta} = \mu r\left.\frac{\partial}{\partial r}\left(\frac{v_\vartheta}{r}\right)\right|_{r=R_o} \tag{39}$$

$$\sigma_{R_o\varphi} = \mu r\left.\frac{\partial}{\partial r}\left(\frac{v_\varphi}{r}\right)\right|_{r=R_o}. \tag{40}$$

The traction exerted by the mantle on the passive plates is on the underside of the passive plates, i.e., $\hat{n} = -\hat{r}$, thus

$$\underline{\underline{\mathbf{t}}}_s \cdot \hat{n} = -\underline{\underline{\mathbf{t}}}_s \cdot \hat{r} = \left(p - \sigma_{rr}, -\sigma_{r\vartheta}, -\sigma_{r\varphi}\right) \tag{41}$$

and the cross product between the radial unit vector and equation (41) near the surface is

$$\hat{r} \times \left(\underline{\underline{\mathbf{t}}}_s \cdot \hat{n}\right) = \left(0, \sigma_{R_o\varphi}, -\sigma_{R_o\vartheta}\right). \tag{42}$$

Substituting equation (42) into equation (34) we obtain

$$\mathbf{T}^{(i)} = R_o^3 \int_0^\pi \int_0^{2\pi} \left(0, \sigma_{R_o\varphi}, -\sigma_{R_o\vartheta}\right) S^{(i)}(\vartheta, \varphi) \sin\vartheta \, d\vartheta \, d\varphi. \tag{43}$$

2.7.3 Shape Functions

We will require a mathematically continuous shape function for our model. The traditional shape function is a step or some simple modification of a step like a ramp or sinc function at a plate boundary. The most simple traditional step function is

$$S^{(i)}(\vartheta,\varphi)=\begin{cases}0, outside\\ 1, inside\end{cases}. \tag{44}$$

The problem with this shape function is that it is mathematically discontinuous and yields infinite traction at the surface (Hager and O'Connell, 1981).

A mathematically continuous plate shape function that is infinitely differentiable and consists of a plate-boundary function for adjusting plate margin widths was developed by Bercovici and Wessel, (1994).

2.7.4 Component Torque Equations

The component torque equations will be developed by using the unit vector equations to perform a transformation from spherical polar coordinates into Cartesian coordinates. These equations are

$$\hat{\vartheta}=\cos\vartheta(\cos\varphi\hat{x}+\sin\varphi\hat{y})-\sin\vartheta\hat{z} \tag{45}$$

$$\hat{\varphi}=-\sin\varphi\hat{x}+\cos\varphi\hat{y}. \tag{46}$$

By substituting equations (45) and (46) into equation (43), we obtain the Cartesian coordinate components of the torque exerted by the driver plates. These equations are

$$T_x^{(i)}=R_o^3\int_0^{\pi}\int_0^{2\pi}\left(\sigma_{R_o\varphi}\cos\vartheta\cos\varphi+\sigma_{R_o\vartheta}\sin\varphi\right)S^{(i)}(\vartheta,\varphi)\sin\vartheta d\vartheta d\varphi \tag{47}$$

$$T_y^{(i)}=R_o^3\int_0^{\pi}\int_0^{2\pi}\left(\sigma_{R_o\varphi}\cos\vartheta\sin\varphi-\sigma_{R_o\vartheta}\cos\varphi\right)S^{(i)}(\vartheta,\varphi)\sin\vartheta d\vartheta d\varphi \tag{48}$$

$$T_z^{(i)}=-R_o^3\int_0^{\pi}\int_0^{2\pi}\sigma_{R_o\varphi}S^{(i)}(\vartheta,\varphi)\sin^2\vartheta d\vartheta d\varphi. \tag{49}$$

To obtain the instantaneous torque on the passive plates, they are held rigid and the torque on them produced by flow induced by the active plates is calculated. The integral

equations (47), (48) and (49) are solved by performing *fast Fourier transforms* in φ and *Gaussian quadrature* in ϑ.

2.8 REFERENCES

Arfken, G., *Mathematical Methods for Physicists*, 3rd ed., 985 pp., Academic Press, Inc., San Diego, 1985.

Bercovici, D. and P. Wessel, A continuous kinematic model of plate-tectonic motions, *Geophys. J. Int.*, **119**, 595-610, 1994.

Chandrasekhar, S., *Hydrodynamic and Hydromagnetic Stability*, 652 pp., Dover Publications, New York, 1981.

Hager, B., and R. O'Connell, Subduction zone dip angles and flow driven by plate motions, *Tectonophysics*, **50**, 111-33, 1978.

Hager, B., and R. O'Connell, A simple global model of plate dynamics and mantle convection, *J. geophys Res.*, **86**, 4843-67, 1981.

Kundu, Pijush K., *Fluid Mechanics*, 638 pp., Academic Press, New York, 1990.

Landau, L. and M. Lifshitz, *Fluid Mechanics*, 2nd ed., Course of Theoretical Physics, Vol. 6, 539 pp., Pergamon Press Ltd., New York, 1987.

Chapter 3

TRACTION AND TORQUE MODELING PROCEDURES

3.1 SUMMARY

The traction vectors will be mapped on a latitude-longitude grid and the effect of the traction produced by the five active plates on the seven passive plates will be determined. The mapping and the torque studies will be done separately for both the free slip bottom boundary (Earth's core) and no slip shallow boundary (660 km discontinuity).

The torque calculated on the five active and seven passive plate model will be compared with the torque calculated on each of the twelve individual plates. The torque calculated on each individual plate is the observable torque. Analogously, the given angular velocity of the observed plates will be compared with the modeled torque of the five active and seven passive plates. These calculations will be accomplished for both the free slip bottom boundary and the no slip shallow boundary cases.

3.2 MODELING PROCEDURES

The traction vector components of equation (41) of section 2.7.2 will be calculated and mapped on a latitude-longitude grid. The calculations will be accomplished by allowing the five active plates of the model to move freely while not allowing any displacement of the seven passive plates.

To determine the effect of the traction produced by the five active plates on the seven passive plates, the Cartesian components of the torque will be calculated by using equations (47), (48) and (49) of section 2.7.4 and by again allowing the five active plates of the model to move freely while restraining the movement of the seven passive plates.

This procedure will result in the determination of the instantaneous torque on the passive plates.

The individual components of the torque produced by each observed plates will be required for comparison with the components of the torque produced by the model of the five active plates on the seven passive plates. The torque for each observed plate is determined by allowing the observed plate to be the only plate that is allowed to move while restraining any displacement of the remaining eleven plates.

3.3 ANALYSIS PROCEDURES

The torque for each observed plate will be compared with the torque for each of the modeled plates. The desired result is a minimal misfit or variance between any observed and modeled torque. In addition to a minimal variance, we want to know if there is a significant directional correlation between the torque vectors of each observed and modeled plate. I.e., are they parallel. The most desirable result is achieved when the variance between an observed and modeled plate approaches zero and the correlation approaches unity (Davis, 1986). The equations for the variance and correlation between each observed and modeled plate are

$$Variance = \frac{\sum_{j=1}^{n}\left(T_{x_j}^{(i)} \Big/ \left|\mathbf{T}^{(i)}\right| - T_{ox_j}^{(i)} \Big/ \left|\mathbf{T}_o^{(i)}\right| \right)^2}{n} \tag{1}$$

$$Torque\ Correlation = \frac{\mathbf{T}^{(i)} \cdot \mathbf{T}_o^{(i)}}{\left|\mathbf{T}^{(i)}\right|\left|\mathbf{T}_o^{(i)}\right|} \tag{2}$$

where $T_{x_j}^{(i)}$ and $T_{ox_j}^{(i)}$ are the torque components of $\mathbf{T}^{(i)}$ and $\mathbf{T}_o^{(i)}$, the torque vectors of each modeled plate and of each observed plate, respectively, $i=1,2,3,....,12$ individual plates, $j=1,2,3$, and x_1, x_2 and x_3 are the x, y and z Cartesian components, respectively.

Lastly, the torque for each of the modeled plates will be compared to the angular velocity of each of the observed plates (DeMets et al., 1990) to calculate the correlation

between the torque and the angular velocity of each modeled and observed plate, respectively. The equation for the correlation is

$$\textit{Angular Velocity Correlation} = \frac{\mathbf{T}^{(i)} \cdot \boldsymbol{\omega}^{(i)}}{\left|\mathbf{T}^{(i)}\right|\left|\boldsymbol{\omega}^{(i)}\right|} \tag{3}$$

where $\boldsymbol{\omega}^{(i)}$ is the angular velocity vector of each of the twelve observed plates. The most desirable result for a modeled torque and observed angular velocity plate set relationship is an angular velocity correlation approaching unity (Davis, 1986).

3.4 REFERENCES

Davis, J.C., *Statistics and Data Analysis in Geology*, 2nd ed., 646 pp., John Wiley and Sons, New York, 1986.

DeMets, C., R. Gordon, D. Argus and S. Stein, Current plate motions, *Geophys. J. Int.*, **101**, 425-78, 1990.

Wessel, P. and W. Smith, *The GMT-System Technical Reference and Cookbook*, 47 pp., Scripps Institution of Oceanography, San Diego, 1992.

Chapter 4

TRACTION AND TORQUE STUDY RESULTS

4.1 SUMMARY

We utilized the model described in the previous chapters to calculate the traction vectors and the torque on each plate for the entire Earth system for both a free slip bottom boundary (Earth's core) and a no slip shallow boundary (660 km discontinuity).

We mapped the traction vectors on a *GMT-System* latitude-longitude grid (Wessel and Smith, 1992) and tabulated the variance and correlation (Davis, 1986) of the observed torque of each individual plate with the modeled torque of both the active and passive plates, and tabulated the correlation of the observed angular velocity (DeMets et al., 1990) of each individual plate with the modeled torque of both the active and passive plates for both the free slip and the no slip boundary cases.

4.2 RESULTS

The traction vector maps of the free slip and no slip boundary cases are found in Figures 4.1 and 4.2 beginning on page 23.

The tabulated results for the observed torque versus the modeled torque for the free slip and no slip case studies are found in tables 4.1 and 4.2 beginning on page 25 and the observed angular velocity versus the modeled torque for the free slip and no slip case studies are found in Tables 4.3 and 4.4 beginning on pages 27.

The histograms for the observed torque versus the modeled torque and the observed angular velocity versus modeled torque for the free slip and no slip case studies are found in Figures 4.3 through 4.5 on page 29.

4.3 REFERENCES

Davis, J.C., *Statistics and Data Analysis in Geology*, 2nd ed., 646 pp., John Wiley and Sons, New York, 1986.

DeMets, C., R. Gordon, D. Argus and S. Stein, Current plate motions, *Geophys. J. Int.*, **101**, 425-78, 1990.

Wessel, P. and W. Smith, *The GMT-System Technical Reference and Cookbook*, 47 pp., Scripps Institution of Oceanography, San Diego, 1992.

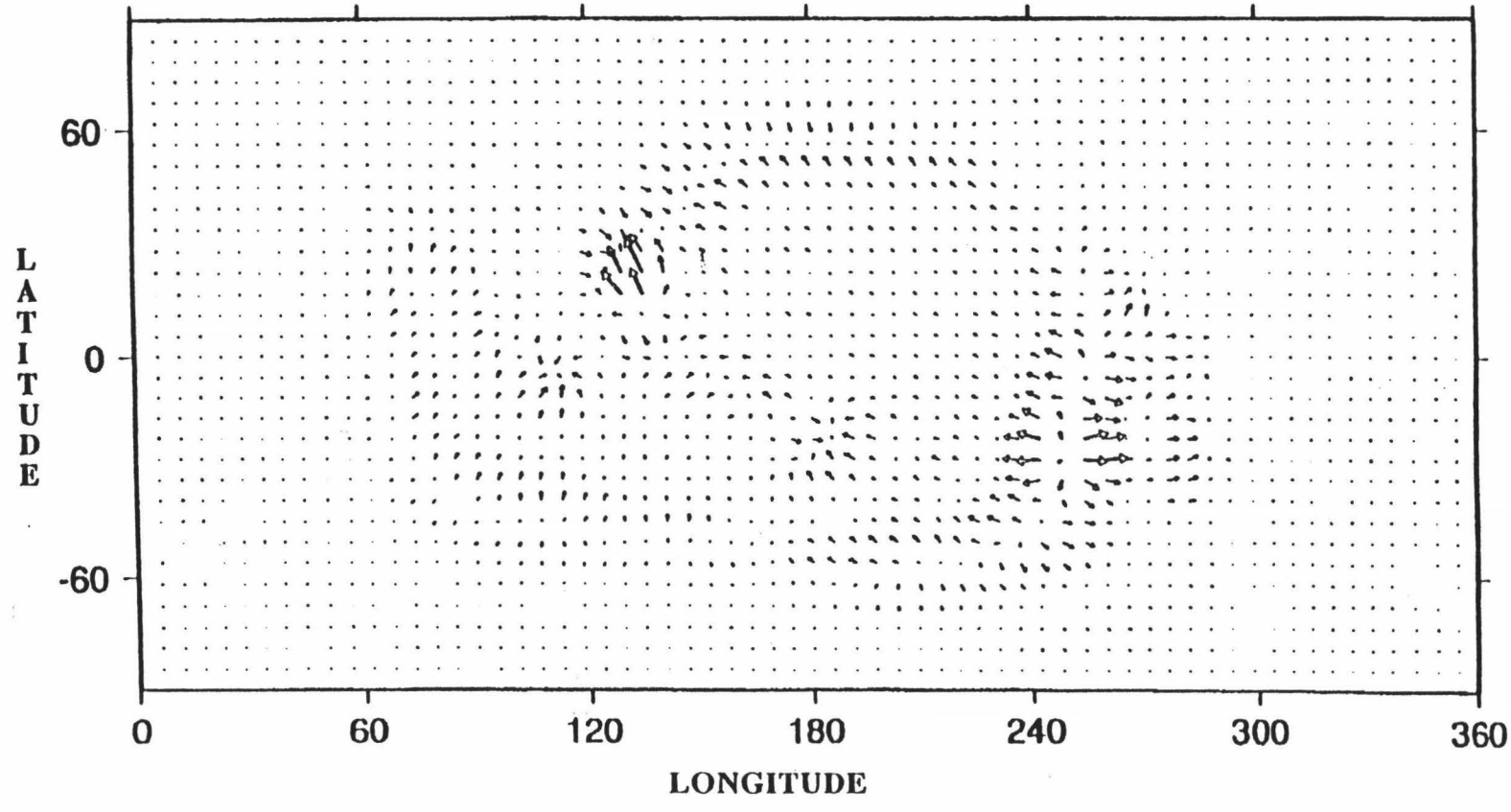

Figure 4.1: Traction Vectors for the Free Slip Core Mantle Boundary (CMB) Case

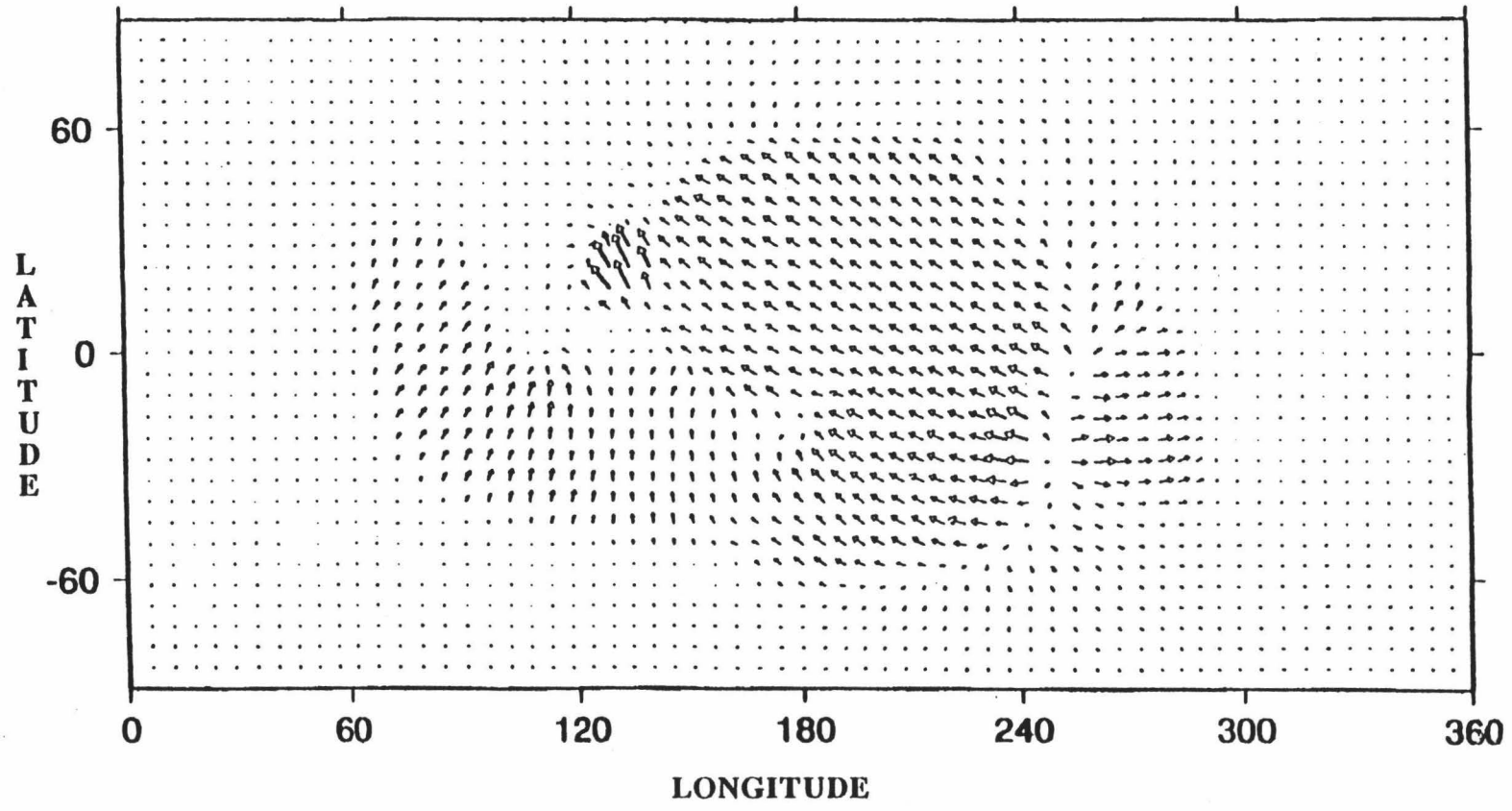

Figure 4.2: Traction Vectors for the No Slip 660 km Boundary Case

Table 4.1: Analysis of Observed and Modeled Torque with a Free Slip Bottom Boundary for Five Active and Seven Passive Plates

Plate and Comp	Observed Torque Each Plate	ModTorque Act. Nonrig Pas. Rigid	Variance	Corr.	Plate and Comp	Observed Torque Each Plate	Mod Torque Act. Nonrig Pas. Rigid	Variance	Corr.
Afr					Ind				
x	10.908752	-6.030585			x	112.266428	129.330448		
y	-9.005970	33.862424			y	54.969103	60.540302		
z	-1.962112	-21.414414			z	42.050265	75.823113		
lvl	14.281395	40.516772	1.045411	-0.568116	lvl	131.884715	161.680665	0.008989	0.986516
Ant					Nam				
x	2.181340	-16.458613			x	19.575342	46.958641		
y	16.880174	54.215079			y	-30.046424	31.095114		
z	-1.002095	-10.965321			z	-31.764639	-14.556551		
lvl	17.050007	57.709609	0.063488	0.904769	lvl	47.905886	58.171413	0.559656	0.160516
Ara					Naz				
x	5.097374	-0.302291			x	-2.942590	0.663601		
y	-4.489827	1.670047			y	-15.462311	-28.395503		
z	-0.119662	-2.161533			z	40.797081	77.819217		
lvl	6.793828	2.748211	0.980184	-0.470276	lvl	43.728065	82.840663	0.001943	0.997086
Car					Pac				
x	0.863889	0.668298			x	-30.506622	-57.129282		
y	-0.486525	0.005334			y	144.982534	143.730279		
z	-3.030494	-0.901203			z	#########	-287.193027		
lvl	3.188559	1.121970	0.050620	0.924070	lvl	312.311434	326.193168	0.002186	0.996722
Coc					Phl				
x	-11.956578	-14.442083			x	24.500631	25.845013		
y	2.016920	3.700193			y	40.488174	34.483241		
z	5.746814	12.595187			z	-36.581909	-21.009216		
lvl	13.418405	19.516761	0.023829	0.964256	lvl	59.814791	47.942109	0.016205	0.975692
Eur					Sam				
x	-1.453796	46.383284			x	-6.065854	4.502225		
y	8.789485	62.138182			y	22.827311	11.987155		
z	-11.954600	-54.550888			z	-55.268513	-9.346228		
lvl	14.909092	94.806972	0.133297	0.800054	lvl	60.103987	15.852883	0.132900	0.800650

Table 4.2: Analysis of Observed and Modeled Torque with a No Slip Bottom Boundary for Five Active and Seven Passive Plates

Plate and Comp.	Observed Torque Each Plate	Mod Torque Act. Nonrig Pas. Rigid	Variance	Corr.	Plate and Comp.	Observed Torque Each Plate	Mod Torque Act. Nonrig Pas. Rigid	Variance	Corr.
Afr					Ind				
x	25.574306	-21.803001			x	243.452647	311.287844		
y	-26.447318	68.805652			y	121.552425	161.557541		
z	-6.338417	-47.511395			z	79.919515	95.826169		
lvl	37.332041	86.411349	1.095729	-0.643593	lvl	283.604147	363.570647	0.000195	0.999707
Ant					Nam				
x	4.206367	-70.267615			x	45.968042	132.196387		
y	39.596899	53.395877			y	-75.033223	39.065771		
z	-1.206318	-13.195374			z	-71.781746	-1.927886		
lvl	39.837961	89.234384	0.322606	0.516090	lvl	113.559080	137.861292	0.526823	0.209766
Ara					Naz				
x	5.415614	-1.242866			x	-4.909966	-7.622288		
y	-4.485116	3.813420			y	-24.524364	-37.245052		
z	-0.609232	-4.234291			z	65.896808	103.213805		
lvl	7.058067	5.832333	1.010889	-0.516333	lvl	70.483626	109.992649	0.000033	0.999950
Car					Pac				
x	0.884704	2.322213			x	#########	-161.247161		
y	-0.496445	-0.104063			y	413.603096	457.186996		
z	-3.113165	-3.130315			z	#########	-829.654844		
lvl	3.274287	3.899022	0.047792	0.928313	lvl	906.484525	960.909859	0.000462	0.999307
Coc					Phl				
x	-9.260936	-14.453444			x	28.534677	31.436289		
y	1.488297	3.229780			y	44.494656	43.223460		
z	4.050491	10.370387			z	-36.697503	-27.921869		
lvl	10.216968	18.079780	0.014639	0.978042	lvl	64.348340	60.300403	0.006070	0.990895
Eur					Sam				
x	-0.628609	33.584232			x	-14.814164	9.946369		
y	22.776615	81.932494			y	48.885623	30.897288		
z	-26.694558	-81.627963			z	#########	-37.418104		
lvl	35.096563	120.432382	0.031972	0.952042	lvl	132.184413	49.534706	0.063409	0.904887

Table 4.3: Analysis of Observed Angular Velocity and Modeled Torque with a Free Slip Bottom Boundary for Five Active and Seven Passive Plates

Plate and Comp	Observed Angular Velocity	Mod Torque Act Nonrig Pass Rigid	Corr	Plate and Comp	Observed Angular Velocity	Mod Torque Act Nonrig Pass Rigid	Corr
Afr				**Ind**			
x	3.096244	-6.030585		x	9.140244	129.330448	
y	-0.314296	33.862424		y	2.968704	60.540302	
z	-0.266889	-21.414414		z	2.732111	75.823113	
lvl	3.123578	40.516772	-0.186475	**lvl**	9.991080	161.680665	0.971295
Ant				**Nam**			
x	1.306244	-16.458613		x	2.434244	46.958641	
y	1.147704	54.215079		y	-0.837296	31.095114	
z	-0.493889	-10.965321		z	-4.528889	-14.556551	
lvl	1.807601	57.709609	0.442306	**lvl**	5.209361	58.171413	0.508844
Ara				**Naz**			
x	9.155244	-0.302291		x	0.562244	0.663601	
y	2.381704	1.670047		y	-6.043296	-28.395503	
z	2.700111	-2.161533		z	5.680111	77.819217	
lvl	9.837764	2.748211	-0.171117	**lvl**	8.312714	82.840663	0.891621
Car				**Pac**			
x	1.978244	0.668298		x	0.585244	-57.129282	
y	-0.613296	0.005334		y	7.988704	143.730279	
z	-2.715889	-0.901203		z	-14.795889	-287.193027	
lvl	3.415499	1.121970	0.982846	**lvl**	16.824988	326.193168	0.977381
Coc				**Phl**			
x	-8.737756	-14.442083		x	12.485244	25.845013	
y	-19.668296	3.700193		y	20.788704	34.483241	
z	7.057111	12.595187		z	-14.795889	-21.009216	
lvl	22.649351	19.516761	0.321916	**lvl**	28.407215	47.942109	0.991550
Eur				**Sam**			
x	1.138244	46.383284		x	1.079244	4.502225	
y	0.421704	62.138182		y	1.342704	11.987155	
z	-1.071889	-54.550888		z	-5.278889	-9.346228	
lvl	1.619376	94.806972	0.895418	**lvl**	5.552863	15.852883	0.798509

Table 4.4: Analysis of Observed Angular Velocity and Modelled Torque with a No Slip Bottom Boundary for Five Active and Seven Passive Plates

Plate and Comp	Observed Angular Velocity	Mod Torque Act Nonrig Pass Rigid	Corr	Plate and Comp	Observed Angular Velocity	Mod Torque Act Nonrig Pass Rigid	Corr
Afr				**Ind**			
x	3.096244	-21.803001		x	9.140244	311.287844	
y	-0.314296	68.805652		y	2.968704	161.557541	
z	-0.266889	-47.511395		z	2.732111	95.826169	
lvl	3.123578	86.411349	-0.283249	lvl	9.991080	363.570647	0.987394
Ant				**Nam**			
x	1.306244	-70.267615		x	2.434244	132.196387	
y	1.147704	53.395877		y	-0.837296	39.065771	
z	-0.493889	-13.195374		z	-4.528889	-1.927886	
lvl	1.807601	89.234384	-0.148710	lvl	5.209361	137.861292	0.414693
Ara				**Naz**			
x	9.155244	-1.242866		x	0.562244	-7.622288	
y	2.381704	3.813420		y	-6.043296	-37.245052	
z	2.700111	-4.234291		z	5.680111	103.213805	
lvl	9.837764	5.832333	-0.239283	lvl	8.312714	109.992649	0.882675
Car				**Pac**			
x	1.978244	2.322213		x	0.585244	-161.247161	
y	-0.613296	-0.104063		y	7.988704	457.186996	
z	-2.715889	-3.130315		z	-14.795889	-829.654844	
lvl	3.415499	3.899022	0.988151	lvl	16.824988	960.909859	0.979350
Coc				**Phl**			
x	-8.737756	-14.453444		x	12.485244	31.436289	
y	-19.668296	3.229780		y	20.788704	43.223460	
z	7.057111	10.370387		z	-14.795889	-27.921869	
lvl	22.649351	18.079780	0.331997	lvl	28.407215	60.300403	0.994870
Eur				**Sam**			
x	1.138244	33.584232		x	1.079244	9.946369	
y	0.421704	81.932494		y	1.342704	30.897288	
z	-1.071889	-81.627963		z	-5.278889	-37.418104	
lvl	1.619376	120.432382	0.821813	lvl	5.552863	49.534706	0.907973

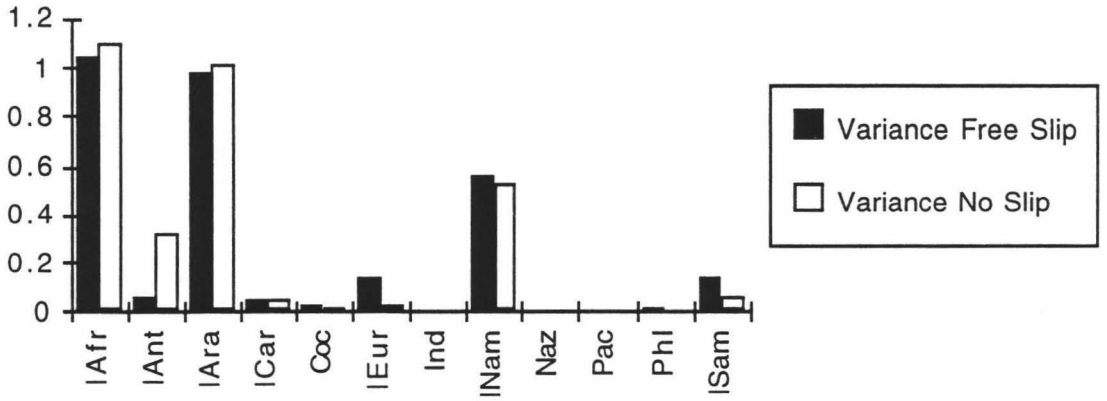

Figure 4.3: Obs. Torque versus Mod. Torque Variance for Free Slip and No Slip Cases

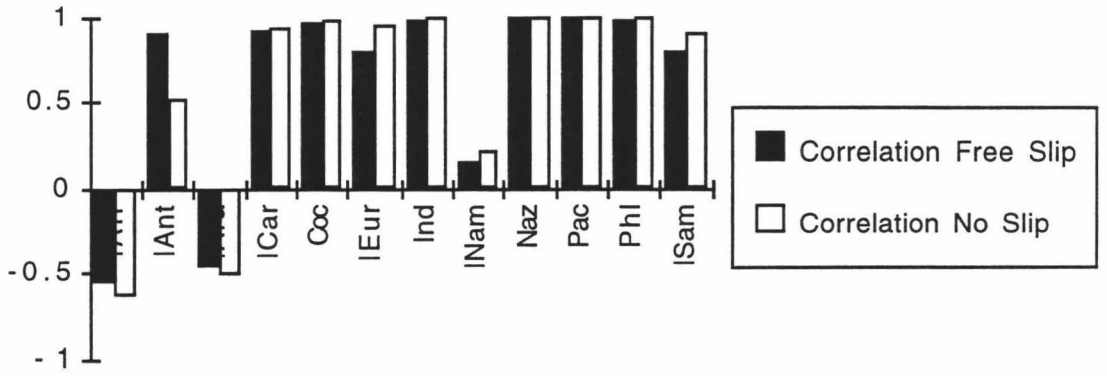

Figure 4.4: Obs. Torque versus Mod. Torque Correlation for Free Slip and No Slip Cases

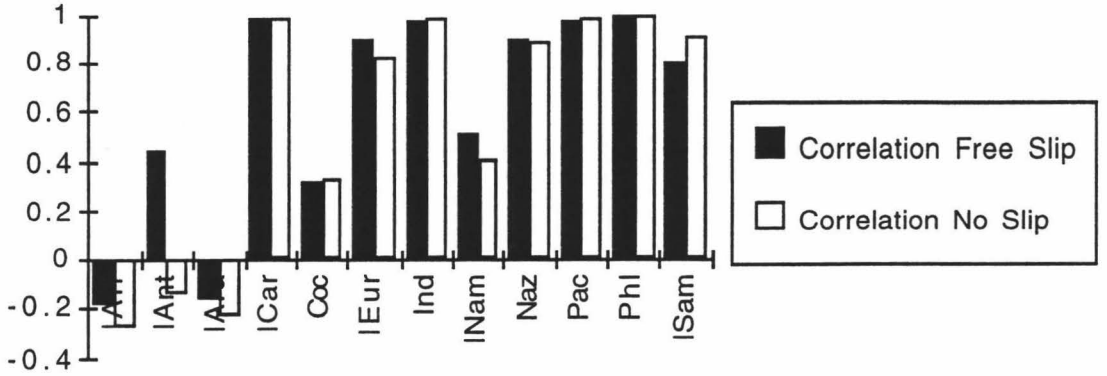

Figure 4.5: Obs. Ang. Vel. versus Mod. Torque Correlation for Free Slip and No Slip Cases

Chapter 5

TRACTION AND TORQUE STUDY DISCUSSION

5.1 SUMMARY

As expected, the variances are a minimum and the torque correlation are a maximum between observed and modeled active plates, with exception of a weak correlation with the observed angular for the Cocos plate. The weak correlation is possibly due to the crude representation of the shape of the Cocos plate model.

Of the seven passive plates, four plates (Antarctic, Caribbean, Eurasian and South American) reveal very good to excellent minimal variances and maximum correlation. In all the studies, the free slip bottom boundary case is favored for the Antarctic plate only. A no slip shallow boundary condition is slightly favored for the European and South American plates and the Caribbean plate favors either boundary. The North American plate is only minimally influenced by the flow induced by the active plates, favors neither a free slip or a no slip boundary. The African and Arabian plates are not influenced at all by flow driven by the active plates.

5.2 THE PLATES

As the tabulated results and especially the histograms illustrate, the variance is a maximum and there is minimal or negative correlation between modeled torque and either observed torque or observed angular velocity for both the African and Arabian plates in both the free slip and the no slip boundary cases.

Neither the African nor Arabian plate are adjacent to any converging margins of active plates. There are some transform faults adjacent to the Indian plate on both of the

plates eastern borders which would not produce enough traction to yield any appreciable torque.

When we examine the Antarctic plate, we find some very interesting results. I.e., The Antarctic plate shows, for the free slip case, a small (.06) variance and a strong (.90) correlation of the observed torque versus the modeled torque, and weak (.44) correlation for the observed angular velocity versus the modeled torque. For the no slip shallow boundary case, there is a moderately large (.32) variance and weak correlation (.52) between the observed torque and the modeled torque, and a negative correlation between the observed angular velocity versus the modeled torque.

We know that the Antarctic plate is fairly slow moving and that the plate margins are either ridges or transform faults without connecting slabs or colliding margins. However, the most interesting result of this study is that the motion of the Antarctic plate is reproducible by our model if the bottom boundary is deep and free slip, but is not reproduced well if the bottom is shallow and no slip.

The Caribbean plate reveals a strong (.92) correlation and a small (.05) variance for both the free and no slip bottom conditions of the observed torque versus the modeled torque studies and there is a strong (.98) and (.99) correlation for the observed angular velocity versus the modeled torque studies for the free slip bottom boundary and the no slip shallow boundary cases, respectively.

The small Caribbean plate receives a northeasterly traction component from the even smaller but very active adjacent Cocos plate's subducting slab and a considerable strong easterly component from the adjacent Nazca plate's subducting slab.

It is impossible to distinguish whether the mantle of the Caribbean plate has a free slip bottom boundary at the Earth's core or a no slip shallow boundary at the 660 km discontinuity. However, some physical intuition regarding the size of the plate would tend to convince us to favor the shallower no slip boundary. The excellent correlation between

observed angular velocity and the modeled torque suggest that the traction from the subducting slabs of the Cocos and Nazca plates do account for much of the motion of the Caribbean plate.

As expected, for the active Cocos plate, the observed torque versus the modeled torque studies reveal a very small (.02) and (.01) variance and a very strong (.96) and (.98) correlation for the free slip and no slip boundary cases, respectively. However the observed angular velocity versus has a weak (.32) and (.33) correlation with both the free slip and the no slip cases.

The very small variance and the excellent correlation between observed and modeled torque for both the free slip and the no slip cases is consistent with the behavior of the other active plates.

Since the Cocos plate is an active plate, we would expect the results of both the observed torque versus the modeled torque and the observed angular velocity versus the modeled torque studies to have a higher correlation. However, the plate is very small when compared to the other active plates and the filtered plate shape is a crude representation of the actual plate shape which possibly explains this discrepancy.

For the Eurasian plate we observe a fair (.13) and very small (.03) variance and a moderate (.80) and strong (.95) correlation for the free slip and the no slip cases for the modeled torque versus the observed torque, respectively. We notice a strong (.90) and good (.82) correlation for the free slip and the no slip cases for the observed angular velocity versus the modeled torque, respectively.

The Eurasian plate is approximately ten percent larger than the Indian plate and slightly greater than half the size of the Pacific plate. The Indian and Pacific active plates both collide with and subduct beneath the Eurasian plate, respectively. The very active Indian and Pacific plates are the apparent prime movers of this very complicated and very old passive plate.

Both studies reveal better than average correlation for a passive plate. However, the observed torque versus the modeled torque studies favor a no slip shallow boundary case and the correlation between observed angular velocity and modeled torque favors a free slip bottom boundary case. An explanation for some erratic behavior may be due to the irregular geometric perimeter of the Eurasian plate. Even though all the Earth's tectonic plates are very thin and relatively insignificant in volume when compared with the asthenosphere and much greater mantle beneath them, some of the passive plates are very old, and possibly much thicker than oceanic lithosphere. Since they carry a significant overburden of mountain ranges. The effects of thick plates are not included in this simple model. These effects could possibly influence the direction of the motion of a real plate. However, accounting for these effects is well beyond the scope of this study.

The Indian plate has a very small (.01) and nonexistent (.00) variance and a reasonably perfect (.99) and (1.00) correlation for the observed torque versus the modeled torque studies and a very strong (.97) to almost perfect (.99) correlation for the observed angular velocity studies for the free slip and no slip boundary conditions, respectively.

Clearly, the Indian plate is a very strong active plate and is not influenced significantly by any of the aforementioned problems peculiar to passive plates or smaller active plates.

When we look to the North American plate, we find a very large (.56) and (.53) variance and very weak (.16) and (.21) correlation between the observed torque and the modeled torque and a moderate (.51) and (.41) correlation between the observed angular velocity and the modeled torque for the free slip and the no slip cases, respectively.

There is considerable traction acting on the North American plate due to the enormous subduction zone delineating the Aleutian Island archipelago. There are some forces due to the asperity of the San Andreas transform fault's extension from the Sea of Cortez, along the plate margin just inside of California's coast range mountains, to the

fault's offshore extension slightly to the south of San Francisco and a transform fault from British Columbia through the inside passage area of Alaska. In addition, there is the complicated triple junction and subducting plate off the coasts of northern California and Oregon which is due to the disappearing Farallon plate. All these features are observed along the margin of the northwesterly migrating Pacific plate (Cox and Hart, 1986).

However, the large variance and apparent lack of correlation between the observed torque and the modeled torque do not tell us whether this plate is actually influenced by the active plates. The slightly larger correlation between the observed angular velocity and the modeled torque indicate a modest case for a free slip bottom boundary.

The Nazca plate and the largest plate on earth, the Pacific plate, reveal an almost perfect (.01) and perfect (.00) variance and a perfect strong (1.00) and (1.00) correlation for the observed torque versus the modeled torque studies for the free slip and the no slip cases, respectively, for both the Nazca and Pacific plates.

The Nazca plate shows a strong (.89) and (.88) correlation between the observed angular velocity and the modeled torque for the free slip and the no slip cases, respectively. The Pacific plate has a very strong almost perfect (.99) correlation between the observed angular velocity and the modeled torque for both the free slip and the no slip cases. These results are expected due to the powerful influences of either active plate. However, unlike the much greater Pacific plate, the Nazca plate is possibly influenced by other plates. This behavior is revealed in the correlation between the observed angular velocity and the modeled torque. Both plates could have either a free slip bottom boundary or a no slip shallow boundary. However, the Nazca plate appears to slightly favor a free slip bottom boundary.

The very active, but reasonably small Philippine plate reveals a very small (.02) and almost nonexistent (.01) variance and a very strong (.98) and (.99) correlation between the observed torque and modeled torque for the free slip and the no slip cases. The

accompanying correlation between observed angular velocity and modeled torque is very strong (.99) for both the free slip bottom boundary and no slip shallow boundary cases.

The Philippine plate exhibits the expected behavior for a strong active plate, i.e., practically no variance and a perfect correlation. The Philippine plate appears to slightly favor a no slip shallow boundary condition.

Lastly, we observe that the South American plate has a moderate (.13) to small (.06) variance and a moderately strong (.80) to a stronger (.90) correlation between the observed torque and the modeled torque and a moderately strong (.80) to stronger (.91) correlation between the observed angular velocity and the modeled torque for the free slip bottom boundary and the no slip shallow boundary cases, respectively.

The South American plate is greatly influenced along the western margin, which is comprised of the entire geographical west coast of the continent, by the subducting slab of the Nazca plate. The evidence for this influence is an enormous trench extending along the entire length of the margin. As the subduction zone of the Nazca plate recedes, the South American plate displaces to the west.

5.3 REFERENCES

Cox, A. and R. Hart, *Plate Tectonics*, 392 pp., Blackwell Scientific Publications, Inc., Boston, 1986.

Chapter 6

TRACTION AND TORQUE STUDY CONCLUSIONS

6.1 SUMMARY

We conclude that in general, the active plates drive the passive plates which are adjacent to an active plate's convergent margin which has a connecting slab and that there is some evidence to support that the Antarctic plate is effected by ridges and/or transform faults of adjacent active plates.

6.2 CONCLUSIONS

We conclude from our studies that traction from the mantle on the Caribbean, Eurasian and South American passive plates resulting from the adjacent convergent margins of the active plates is responsible for the observed motion of these plates at the Earth's surface. The Caribbean plate is affected by the Cocos and Nazca plates, the Eurasian plate is affected by the Indian, Pacific and Philippine plates and the South American plate is affected by the Nazca plate. The Caribbean plate does not significantly favor a free slip or a no slip boundary. A no slip shallow boundary may be favored for the Eurasian and South American plates.

Even though there are no subducting slabs adjacent to the Antarctic plate, it gives all appearances of being influenced by the transform faults and/or the ridges of the Indian and Pacific plates for the free slip bottom boundary case only.

The North American plate, though adjacent to the Pacific plate's subducting slab, which extends along the width of the Aleutian trench, is only moderately affected by the Pacific plate's subducting slab. Perhaps, because of the enormity and complexity of the North American plate, in addition to it's orientation with respect to the Aleutian trench,

which is orthogonal to most of the length of the plate, the area effected by the Pacific plate's motion is not significantly large enough to influence the North American plate's motion.

We conclude that the African and Arabian plates, which are not adjacent to the converging margins of any active plate, are not affected by the active plates in a significant way and that their modeled motion can be treated as noise.

6.3 FUTURE STUDIES

In our study we utilized data that was collected and analyzed from the late 1970's through 1990 (Minster and Jordan, 1980; Pollitz, 1988; DeMets et al., 1990). Since then, much more detailed data has become available.

Recently, declassified U.S. satellite and European spacecraft data has been released showing much more complete seafloor detail than has previously been available from oceanic surveys in research vessels (DeMets, et al., 1994; Monastersky, 1995).

6.4 REFERENCES

DeMets, C., R. Gordon, D. Argus and S. Stein, Current plate motions, *Geophys. J. Int.*, **101**, 425-478, 1990.

DeMets, C., R. Gordon, D. Argus and S. Stein, Effect of recent revisions to the geomagnetic reversal time scale on estimates of current plate motions, *Geophys. Res. Ltr.*, **21**, 2191-2194, 1994.

Minster, J., and T. Jordan, Present-day plate motions, *J. geophys. Res.*, **83**, 5331-54, 1978.

Monastersky, R., A new view of Earth, *Science News*, **148**, 410-411, 1995.

Pollitz, F., Episodic North America and Pacific plate ,motions, *Tectonics*, **7**, 711- 26, 1988.

Chapter 7
REFERENCES

Arfken, G., *Mathematical Methods for Physicists*, 3rd ed., 985 pp., Academic Press, Inc., San Diego, 1985.

Bercovici, D. and P. Wessel, A continuous kinematic model of plate-tectonic motions, *Geophys. J. Int.*, **119**, 595-610, 1994.

Bercovici, D., G. Schubert, and G. Glatzmaier, Three-dimensional spherical models of convection in the Earth's mantle,*Science*, **244**, 950-955, 1989.

Chandrasekhar, S., *Hydrodynamic and Hydromagnetic Stability*, 652 pp., Dover Publications, New York, 1961.

Cox, A. and R. Hart, *Plate Tectonics*, 392 pp., Blackwell Scientific Publications, Inc., Boston, 1986.

Davis, J.C., *Statistics and Data Analysis in Geology*, 2nd ed., 646 pp., John Wiley and Sons, New York, 1986.

DeMets, C., R. Gordon, D. Argus and S. Stein, Current plate motions,*Geophys. J. Int.*, **101**, 425-478, 1990.

DeMets, C., R. Gordon, D. Argus and S. Stein, Effect of recent revisions to the geomagnetic reversal time scale on estimates of current plate motions, *Geophys. Res. Ltr.*, **21**, 2191-2194, 1994.

Forsyth, D. and S. Uyeda, On the relative importance of the driving forces of plate motion, *Geophys. J. R. astr. Soc.*, **43**, 163-200, 1975.

Hager, B., and R. O'Connell, Subduction zone dip angles and flow driven by plate motions, *Tectonophysics*, **50**, 111-33, 1978.

Hager, B., and R. O'Connell, A simple global model of plate dynamics and mantle convection , *J. geophys Res.*, **86**, 4843-67, 1981.

Kundu, Pijush K., *Fluid Mechanics*, 638 pp., Academic Press, New York, 1990.

Landau, L. and M. Lifshitz, *Fluid Mechanics*, 2nd ed., Course of Theoretical Physics, Vol. 6, 539 pp., Pergamon Press Ltd., New York, 1987.

Minster, J., and T. Jordan, Present-day plate motions, *J. geophys. Res.*, **83**, 5331-54, 1978.

Monastersky, R., A new view of Earth, *Science News*, **148**, 410-411, 1995.

Pollitz, F., Episodic North America and Pacific plate ,motions,*Tectonics*, **7**, 711-26, 1988.

Wessel, P. and W. Smith, *The GMT-System Technical Reference and Cookbook*, 47 pp., Scripps Institution of Oceanography, San Diego, 1992.